Spectrochimica Acta Part A: Molecular and Biomolecular Spectroscopy 239 (2020) 118435

Contents lists available at ScienceDirect

Spectrochimica Acta Part A: Molecular and Biomolecular Spectroscopy

journal homepage: www.elsevier.com/locate/saa

Microfluidic approach for controlled ultraviolet treatment of colored and fluorescent dissolved organic matter

R. Lopes [a,b,*], M.L. Miranda [b,c], H. Schütte [a], S. Gassmann [a], O. Zielinski [b,d]

[a] Jade University of Applied Sciences, Department of Engineering, Wilhelmshaven, Germany
[b] Carl von Ossietzky Oldenburg University, ICBM, Wilhelmshaven, Germany
[c] Laboratorio de la Calidad del agua y Aire (LACAYA), Universidad de Panamá, 0824 Panamá, Panama
[d] Marine Perception Research Group, German Research Center for Artificial Intelligence (DFKI), Oldenburg, Germany

ARTICLE INFO

Article history:
Received 26 July 2019
Received in revised form 28 April 2020
Accepted 28 April 2020
Available online 1 May 2020

Keywords:
Microfluidics
FDOM
HIX
CDOM
Slopes
EEMS
Aquatic systems

ABSTRACT

Using microfluidic systems to address the optical properties of Colored and Fluorescent Dissolved Organic Matter (CDOM/FDOM) offers new ways for researching its interactions with the environment, and its response to rapid, as well as extreme, changes of abiotic conditions. Here we present a microfluidic device with an Ultraviolet (UV) component. The manufactured microfluidic device consists of passing a dissolved organic matter sample through a microchannel applying a combination of treatments using different UV wavelengths and exposure times. Here we test the workability of the microdevice by analyzing the effect of UV light on CDOM and FDOM, using as irradiations UVA and UVB to incite photodegradation, over different times. We then compare the absorbance and fluorescence, measured from both treated and non-treated samples. The analysis of the measurements is done by the calculation of the slope ratio, as indicative of molecular weight and dissolved organic carbon, besides the fluorescence humification index (HIX) as an overview of the difference between treated and non-treated of the excitation-emission matrices (EEMs). Our results show the efficiency of the microdevice by demonstrating a direct relation of degradation degree with exposure time. FDOM exposure to UVB shows a possible relation to humic-like fluorophores intensity, shown in HIX and the overview difference. Furthermore, the changes showed in the slope ratio demonstrate photodegradation in all treatments, with UVB exhibiting an increased influence. The combination of microfluidic sample treatment within in situ applications of optical sensors will enhance our capacities in addressing biogeochemical processes in the marine environment, which were not accessible with conventional bulk methods.

1. Introduction

Microfluidics is a technology and a study of fluids in the microscale or smaller. The presented system uses miniaturized fluidics for the creation of controlled highly reproducible conditions under strict laminar flow. Regarding its size, it is with 1 mm channel width at the edge of the definition of microfluidics, but we have guaranteed that the typical microfluidics conditions apply. Therefore, and due to the lack of clear a definition of the next bigger size scale in fluidics, we named our system microfluidics [1–4]. This technology has gained some ground in many areas, such as chemistry, biochemistry, biomedical devices and applications, for its characteristics, such as high resolution and sensitivity, low costs, small sample volume and analysis time [3,5]. Because of these advantages, microfluidics is already being adapted to marine science research. Shen et al. [50] developed a microfluidic-chip-based capillary gel electrophoresis with laser-induced fluorescence detectors, to characterize dissolved organic carbon in environmental water. Gassmann et al. [47] created a microfluidic system with the intent of treating natural samples with temperature gradients, using two temperature zones with a range from 4 °C to 20 °C for the cold zone, and 20 °C to 90 °C for the hot zone so that the sample would cycle between zones in a user-determined time and cycles. Herein we utilized this system and adapted it to integrate a UV LED illumination as an additional treatment.

This adaptation was representative of the sun's ultraviolet (UV) radiation, which directly interacts with the water column, influencing the carbon cycle of the sea. However, the UV radiation needs to pass through the ozone layer, which reduces the availability of the bandwidth of UV reaching the ocean. With this in mind, only 50% of UVA (315 nm to 400 nm) and 10% of UVB (280 nm to 315 nm) can interact with the water column. UV radiation and temperature are two factors affecting dissolved organic matter (DOM). Colored dissolved organic

* Corresponding author at: Jade University of Applied Sciences, Department of Engineering, Wilhelmshaven, Germany.
E-mail addresses: raquel.lopes@jade-hs.de (R. Lopes), mario.luis.miranda.montenegro@uni-oldenburg.de (M.L. Miranda), helmut.schuette@jade-hs.de (H. Schütte), stefan.gassmann@jade-hs.de (S. Gassmann), oliver.zielinski@uni-oldenburg.de (O. Zielinski).

https://doi.org/10.1016/j.saa.2020.118435
1386-1425/

matter (CDOM) is a substantial part of DOM, both in fresh- and seawater, having a strong influence on the subsea optical conditions [6,7]. Through selected absorption of lower wavelengths, it limits light availability for photosynthesis, at the same time protecting it from harmful UV irradiation [8,9]. This process also causes an effect known as photobleaching, which involves CDOM decomposition and production of carbon dioxide, as well as several small organic molecules, the later as a potential carbon source for microbes [10]. Then we have fluorescent dissolved organic matter (FDOM), a fraction of CDOM that emits photons of different wavelengths that is used as a tracer of DOM changes [11,12]. FDOM fluorescence intensity decreases with the increase of temperature as a result of quenching[13,14]. DOM typical composition includes lignin, humic and fulvic substances, proteins and amino acids residues. However, molecular weight and composition can differ according to the geographical location, local development of human activities and industries [13,15].

Two tools to characterize CDOM and FDOM optical properties, used in the laboratory, are the ultraviolet-visible absorption spectra and excitation-emission matrix spectroscopy (EEMS). The UV–visible absorption spectra of CDOM exhibits an exponentially increase when reaching the lower wavelengths, which, by analyzing the ratio of absorption at 250 nm to 365 nm and 465 nm to 665 nm, serves as an indicator for molecular weight, molecular size, O:C and C:N atom ratios, carboxyl content and total acidity [16,17]. Besides, the investigation of its slope of two distinct regions, 275–295 nm and 350–400 nm, and its slope ratio can be used as a proxy for dissolved organic carbon (DOC) and CDOM molecular weight [16]. Furthermore, the fluorescence-based EEMS also gives valuable information, such as organic matter dynamics, composition, concentration, and distribution [8,18]. This technique measures the three-dimensional fluorescent spectra of FDOM compounds over a pre-defined wavelength range [19,20]. According to the location of specific peaks in excitation-emission matrices (EEMs), it is possible to describe the main composition, source and transformations of DOM in the samples [8]. In the FDOM characterization, three indices can be valuable, the humification index (HIX), the biological index (BIX) and the relative contribution of recently produced DOM (REPIX) [11,21]. HIX gives the relative degree of humification, where the C/H ratio can also provide the DOM maturation [22,23]. BIX is used to determine the biological origin of the components and REPIX uses protein-like, humic-like and marine humic-like fluorophores to indicate the manifestation of freshly formed DOM [11,24,25]. Apart from laboratory instrumentation, in situ sensors for ship-based applications and autonomous operations are rapidly developing [20,26,27]. Spectral absorption and therefore CDOM can be derived utilizing reflective tubes or spheres [20,28,29]. Multi-wavelengths FDOM sensors are commercially available, even though they are, strictly speaking, sampling the particulate and dissolved fraction of DOM [30,31]. Recently, a submersible full EEMS sensor was presented by Zielinski et al. [51].

The designed microfluidic system creates a controlled and highly reproducible conditions while reducing the time needed for the transformation caused by UV radiation on DOM; helping to understand the CDOM/FDOM changes induced by the exposition to a combination of temperature and UV irradiation. We aim to understand the difference between the individual treatments and the combined effect of UVA and UVB on the sample while controlling temperature to avoid heating from the LEDs. The overall aim of this research is to show the feasibility of such a novel approach and to showcase the changes caused by UV radiation on CDOM and FDOM, using a microfluidic device and water from natural samples. Specifically, our objectives are i) to present the design of a novel UV irradiation extension to the microfluidic treatment system. ii) prove the UV microfluidic systems efficiency. iii) examine the dependence of photodegradation on different treatment times and UV irradiations.

2. Materials and methods

2.1. Chip development

Gassmann et al. [47] produced a microdevice design to heat and cool a sample using a printed circuit board as a base (PCB). The designed PCB has two squared sides, which were named as cold and hot zone, and underneath each of them, a pocket was milled to have a good thermal transmittance between the channel and the Peltier Elements. The micro-milled polymer channel was also planned to keep the sample on top of the PCB squares and is glued with acrylic glue to the PCB. After the results of the microdevice prototype were tested in the channel was adapted to the current state. Some issues had to be improved due to the contamination of the sample by the materials. In this study, they detected that the polymer and the acrylic glue were big factors in the leaching, which would increase with a DOM sample; for that reason, the microchannel is now milled with Polymethyl methacrylate (PMMA) also known as PLEXIGLAS ®. To avoid contact of the sample with the acrylic glue, a solvent bonding technique was used to unite two pieces of PMMA, with different thicknesses (PLEXIGLASS ® XT Clear 2 mm and PLEXIGLASS ® Film 99,524 0.5 mm from Evonik Performance Materials GmbH). Allowing the usage of the acrylic glue to link the PCB to the PMMA channel [32,33]. The material was then tested in Lopes et al. [32], using the same treatments as Miranda et al. [15] and no leaching was detected. In addition to the material of the channel, the sample volume was changed to undertake at least 100 μL volume from the used cuvettes. This was accomplished by increasing the depth to 1 mm, allowing the treatment of 120 μL sample volume. Due to the changed size, the channel is now in between definitions, however, since the maximum used flow rate is 500 μL/min, the flow behavior is laminar with a Reynolds number < 10, and we consider that it is still within the microfluidic definition. Another addition was the UV LEDs (DUV-HL5NR, Roithner LaserTechink GmbH) to the chip, so the “LED board” was produced, which can be added or removed from the chip, thus it is supported and connected to the PCB with pinheads, which also give the adequate height for the LEDs to be focused (Fig. 1). This change showed the necessity of modifying the PMMA and the temperature program used, allowing both sides to warm or cool as needed. We used PLEXIGLAS® XT Clear 0A770 UV transmitting from Evonik Performance Materials GmbH to enable the UV light to come through. This PMMA has a different transmittance for the selected wavelengths of the LEDs, with 57% for the 280 $\pm$ 5 nm, UVB zone, and 87% for the 340 $\pm$ 5 nm, UVA zone. The LED's higher incidence focus has a 5 mm diameter, which irradiated about 11% of the sample volume. For that reason, on either side, the sample is programmed to be in constant movement, to allow the irradiation of the entire sample.

A self-made C# program for the syringe pump ensures the movement of the sample inside each side of the channel, by controlling the flow rate and direction of the liquid, therefore defining the type, amount and time of cycles, i.e., the treatment. For temperatures, however, an outside controller with an LCD is used: here the temperatures are displayed and defined, this component shows a real-time reading of the current temperature inside the channel (Fig. 2).

2.2. Sample collection, handling, treatments and procedures

Samples were taken from the Jade Bay (53.4500°N 8.2000°E) located in the southern North Sea. Its composition includes different terrestrial and marine sources. On the 7th of May 2018, around 10 am, with low tide, a sample was collected on Jade Bay and filtered, with a nominal pore size of 0.2 μm with a Nucleopore® membrane, later stored in a glass container covered in aluminum at 4 °C.

The sample was tested in the microfluidic device, using three main treatments setups UVB, UVA or a combination of UVA followed by UVB (combined). In each of the main treatments, we tested four different times, keeping the temperature at 20 °C for all the treatments. The

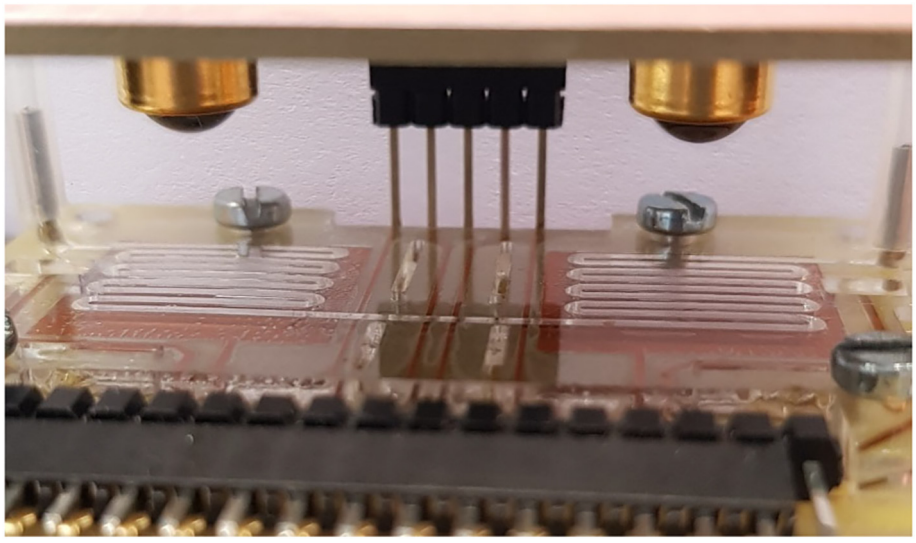

Fig. 1. - Close up of the microchips and channel. On top, it is shown the two LED's (340 nm on the left and 280 nm on the right) centered on top of each side of the channel. One of the three pinheads (center of the picture) that are used as support and connection of the LED board to the PCB. The PCB drawing where the two squares that delimitate the different zones of temperature and the milled channel on top. In the bottom another set of connectors, where the link between the PCB and the supporting electronics is. The screws connect the PCB and channel to the Peltier Elements. On both sides, the channel is centered on top of both square cooper zones of the PCB, which is warmed or cooled with the Peltier Element, as the connections to the mainboard.

times used were 15, 30, 60 and 90 min. For the combined, we would have 15 min in the UVA followed by 15 min in the UVB, and the same for the other times.

To prepare the setup of each treatment, after washing the channel, we rinsed it with a small amount of sample, to avoid dilution by the purified water leftovers from the washing, followed by air. Both syringe and the tube were filled with the sample to function as propelling liquid, leaving about 0.2 mL of space to later collect the sample. The UV LED system is turned ON (Fig. 2), and the temperature is defined to verify the system stability. In the created program, we set the option of "Fill

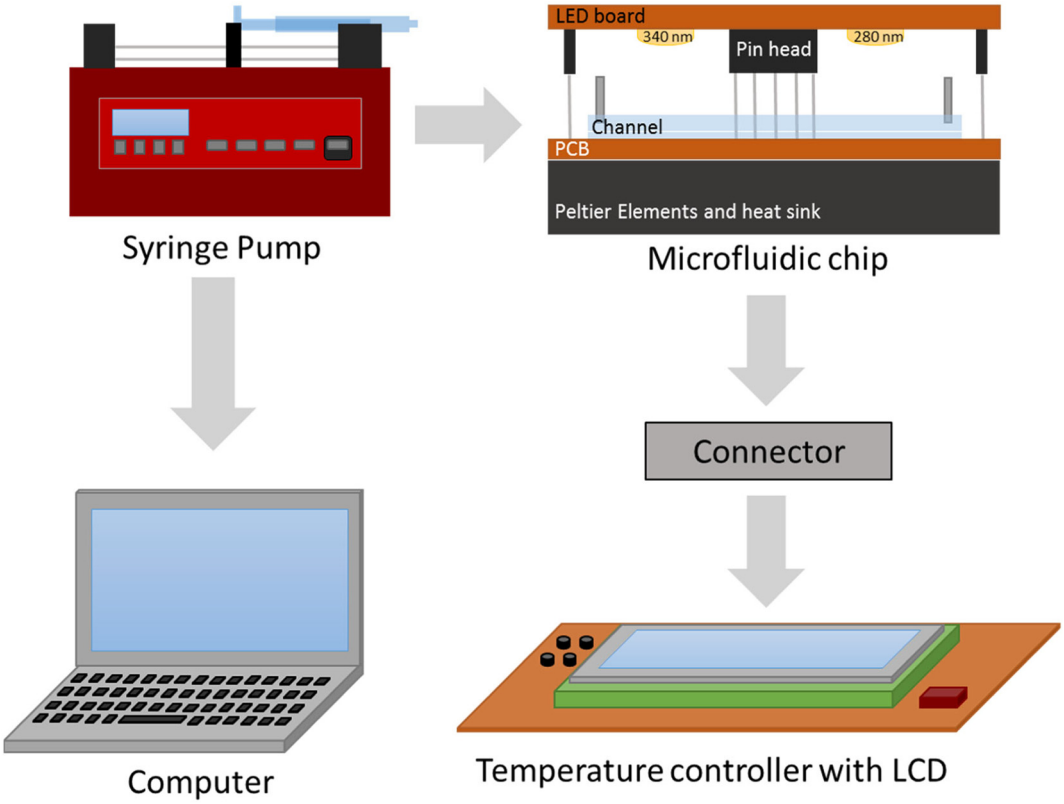

Fig. 2. - System schematic. From left to right, we have the syringe pump controlled by a self-produced software, which is responsible for the movement of the sample inside the channel. The channel is glued to a PCB, which is pinned to the LED board, the connector and screwed to the Peltier Elements. The connector has two jumpers that allow turning on/off the LEDs, two potentiometers to regulate/fix the temperature, and it is linked to the temperature controller. The temperature controller has an LCD where we can see in real-time the temperature and has buttons to regulate it. Two different power supplies provide current to Both Peltier elements and the temperature controller.

Sample", to predefine the amount of sample taken by the syringe pump. According to this setup, the propelling liquid is first pushed in to assure it is on the tip of the tube, then a cushion of air is withdrawn to separate the sample from the propelling liquid. The program informs the user to place the tube to recoil the sample after the user authorization the sample is collected, followed by another withdrawn cushion of air, to prevent the sample to be on the tip of the tube. Then the time and type of treatment are defined, the tube is inserted in the input of the channel, which by default is always in the UVA side, the "Run" button must be pressed to initiate the treatment. The time, zone and constant movement of the sample in the channel is controlled by the syringe pump, ensuring the complete irradiation of the sample.

Since the default setup sample always initiates in the UVA zone, the combined treatment always starts by passing through this zone for the designated time with a constant movement, followed by the sample transference into the UVB zone and the application of the same testing condition but with the complementary UVB source. To avoid cross-contamination, the channel cleanliness was verified each time by obtaining treated blanks. These blanks were obtained by using only purified water as transport liquid and sample, the fluorescence was measured with LS55 Spectrofluorometer (PerkinElmer, USA).

The collected sample is subjected either to one of the treatments or directly measured, attaining two sets of measured samples, treated and non-treated samples. Samples absorptions were first measured with a UV-VIS spectrophotometer (UV-2700, Shimadzu, Japan) within a range from 200 to 600 nm, followed by the measurement of the fluorescence spectra with an LS55 Spectrofluorometer (PerkinElmer, USA). EEMS were recorded using the following setup: Energy high gain (900 V), emission range from 200 to 600 nm, and an applied excitation wavelength ranged from 200 to 400 nm, with 5 nm step. Samples were analyzed by triplicates, except for the combined 60 min and combined 90 min, which were limited to two repetitions each.

2.3. Data calculation and processing

Data was transferred from the user interface into Excel sheets manually. Obtained data was processed with a self-made MATLAB script, which analyzes, calculates and plots different parameters, using the acquired data from the spectrometer and spectrofluorometer. All calculations, plots and statistical were done in MATLAB 2017a (The MathWorks, USA).

2.3.1. Slope ratio

Absorption spectrum was measured in a 10 mm quartz cuvette (16.100-Q-10/Z15 from Starna, England). Slope calculations were done according to Green & Blough [34] and, Eq. (1).

$$a_{CDOM(\lambda)} = 2,303 \times A(\lambda)/l \quad (1)$$

where $a_{CDOM(\lambda)}$= Napierian absorption coefficient (m^{-1}), $A(\lambda)$= absorbance, l= cuvette path length (m), λ=wavelength (nm) [34]. Data is smoothed, by the *smooth* function from MATLAB using an average filter. We obtain the spectral slopes (S, nm^{-1}) values, by applying Eq. (2), accordingly with, here the reference wavelength (nm) is represented by λ0.

$$S = \frac{-\log\left(\frac{a_{CDOM(\lambda)}}{a_{CDOM(\lambda 0)}}\right)}{(\lambda 0 - \lambda)} \quad (2)$$

To obtain the slope ratio two S were calculated after dividing the spectra into two distinct regions, $S_{275-295}$ for the shorter wavelength region and $S_{350-400}$ for the longer wavelength region using the Napierian absorption coefficient from wavelengths 275, 295, 350 and 400 nm and respective wavelengths, to obtain the S values of each region. Here the 275 nm and 350 nm are used as the reference wavelength (λ0), while 295 nm and 400 nm are used as λ, respectively. From both slopes, we then calculated the slope ratio by dividing the slope of the shorter wavelengths by the slope of the longer wavelengths region. Using its averages, we then analyze the different treatments over time, this can show a DOM and a photochemical shift in the molecular weight [16,21]. Helms et al. [16], Li and Hur [17] and Hansen et al. [36] use the linear fitting to understand the trending of the results over time and correlate it with photo and/or biodegradation.

2.3.2. Treated and non-treated EEMS subtraction

EEMS spectra were used to follow up changes in the FDOM fingerprint due to the UV irradiation for both treated and non-treated samples. Using EEMS data, we calculated the averages of the treated and non-treated samples, the background was corrected by subtracting blanks in each treatment. This operation removes Rayleigh and Raman scattering lines Fig. 3 a,b. The result of this operation is two new matrices, subtracted from each other, represented as surface plots, Fig. 3. However, this procedure would give a general idea of the EEMS composition, but it will not show the main differences between treated and non-treated samples. Therefore, non-treated samples were subtracted from the treated and vice versa. The results were two images in which is clearly depicted the fundamental differences between treated and non-treated samples, Fig. 3 c,d. As can be seen in Fig. 3c, the subtraction of the non-treated from the treated samples fluorescent intensity (FI) shows a missing peak, after the UV treatment; while Fig. 3d shows a newly produced peak, after applying the UV treatment. This subtracting process helps to understand and visualize the dynamics of the DOM reprocessing and transformations under UV irradiation.

In Fig. 3b, the non-treated sample EEMS shows a peak located in a specific position defined by the pair of emission/excitation wavelengths (EM/EX) = 350/225 nm. This peak is isolated after the subtraction process, Fig. 3d. On the other hand, the treated sample EEMS (Fig. 3a), shows a slightly different composition compared to the non treated sample (Fig. 3b), but once the subtraction is performed, a peak located at (EM/EX) = 500/220 nm is isolated, Fig. 3c. This method does not completely remove scattering lines, but still produces results that show main changes in EEMS composition due to the UV treatments.

2.3.3. HIX

The humification index is calculated from the H/L ratio, first presented by Zsolnay et al. [35]. Consisting of two zones of the emission spectra at excitation of 254 nm, zone H is obtained by the sum of fluorescence intensity between 435 nm and 480 nm, while zone L is acquired by the sum of fluorescence intensity between 300 nm and 345 nm, shown in Eq. (3).

$$HIX_{254} = \frac{\sum(435-480nm)}{\sum(300-345nm)} = \frac{H}{L} \quad (3)$$

The increase of HIX is directly related to a high aromaticity degree in DOM. Values of HIX higher than 10 indicate a terrigenous contribution with a strong humic character. Between 6 and 10, the components have an important humic character with weak recent autochthonous components. From 4 to 6 the humic character is weak while there is an important recent autochthonous component, whereas values inferior to 4 can show aquatic bacterial or biological origin [25,35].

3. Results

3.1. Slopes, slope ratio

Based on the absorption data, we calculated the high molecular slope ($S_{350-400}$), and the low molecular slope ($S_{275-295}$) to be able to obtain the slope ratio ($S_{275-295}/S_{350-400}$). Our results indicate that changes in the slope ratio are related to the UV source and the irradiation time.

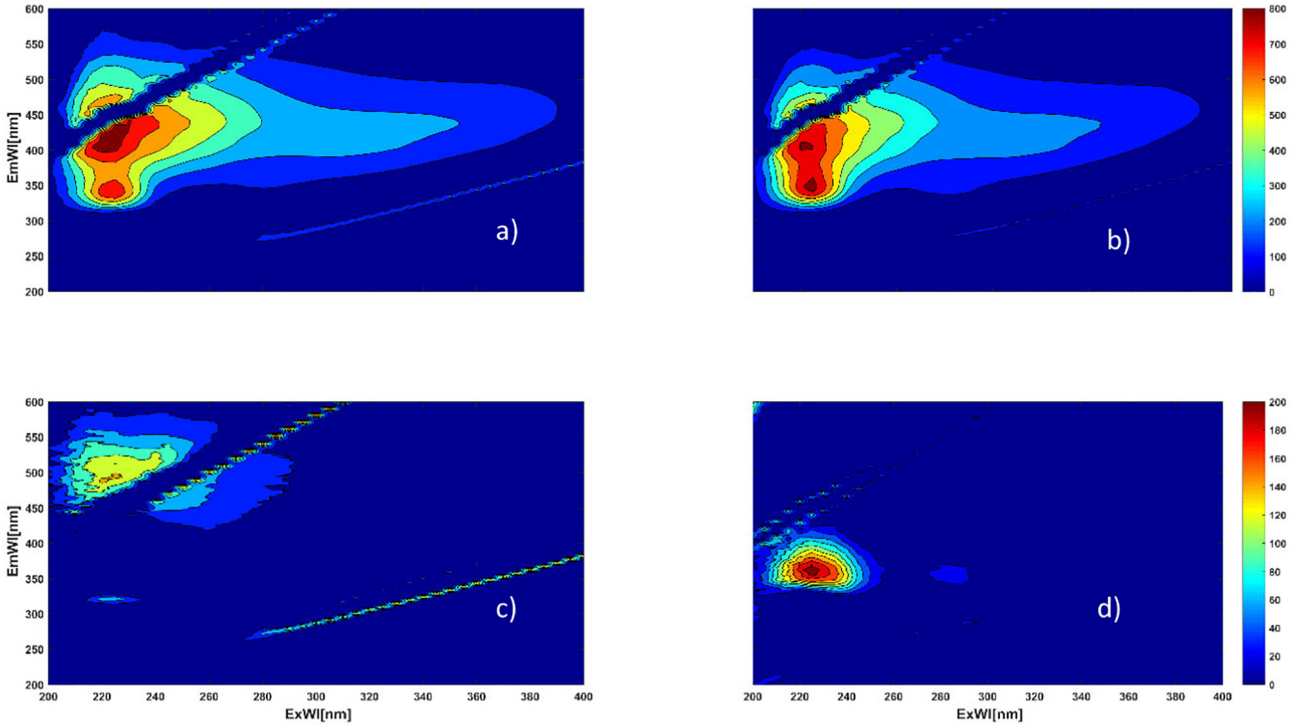

Fig. 3. - Results of the treatment with UVA for 60 min. a) Average of treated samples with the background removed; b) the average of non-treated samples with background removed followed by the color bar [0 to 800] representing the first two images; c) represents subtraction of the fluorescent intensity of non-treated from treated samples, negatives values are removed; d) represents the subtraction of the fluorescent intensity of treated samples from non- treated samples, negative values are removed. The color bar in arbitrary units (A.U.).

This feature has previously been correlated to the concentration of dissolved organic carbon [16].

As it is shown in Fig. 4, by applying selected setups, our device can induce an increase of the slope ratio in the treated samples, proving the efficiency of the microfluidic device as a vehicle to modify the CDOM/FDOM samples characteristics. Simultaneously, we confirmed that even the shortest treatment setups exert a unique influence on CDOM/FDOM profiles when compared with the non-treated samples. As referred to previously, the data analysis were accomplished by a trending line over time using linear fitting [16,36]. To analyze the changes in the slope ratio values, we fitted a curve using the slope ratio as a function of time. A linear fitting of the curve for all treatments is presented, each point represents the average value of each type of treatment data point, and we note that non-treated (NT) slope values

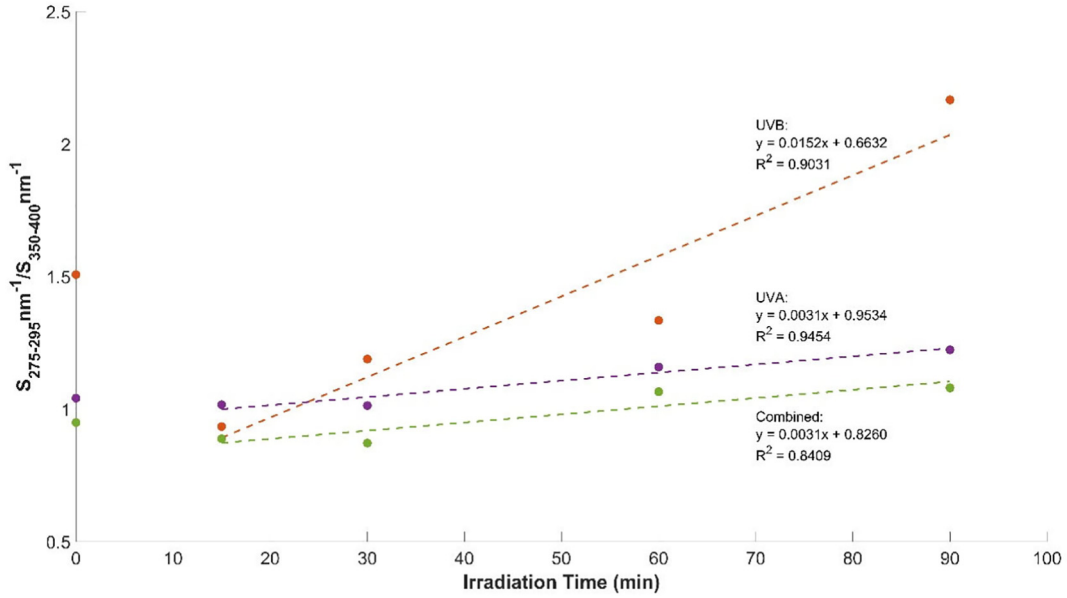

Fig. 4. - Spectral slope ratio. For each treatment there is a NT sample, in the irradiation time at 0 min, measured on the same days the respective treatments occurred. For each treatment, a linear fitting is presented concerning time. UVB is represented by red, UVA by green and combined by blue. (For interpretation of the references to color in this figure legend, the reader is referred to the web version of this article.)

were chosen as treatment time zero ($t = 0$ min), Fig. 4. The linear fittings of each treatment over time showed an R^2 higher than 0.9 for UVA and UVB, with the lower R^2 equal to 0.86 for the combined treatment. This R^2 value in the combined treatment is explained by the higher variability in its behavior, which is influenced by the use of both UVA and UVB irradiation sources, resulting in a similar profile as the UVA treatment. We used the NT slope ratio average of each treatment as a treatment time zero ($t = 0$), with the overall average being 1.15. The slope ratio values of NT used to fit the curves tend to be slightly higher than the 15 min mark on all treatments, however, in all cases, there is an increase in the linear fitting from 15 until 90 min; UVA and combined treatment show similar behaviors with a difference of 0.0001 in the slope of the linear equation and the equation interception in y coordinate.

The increase in the slope ratio when applying the UVB setup suggests that photodegradation is happening in the sample, correlating it directly to irradiation time. This agrees with previous reports indicating an accentuated effect of UVB on DOM mineralization [16]. Thus, indicating that the molecular weight of DOM decreases over time, i.e., a shift from high to low molecular weight.

3.2. Treated and not treated EEMS subtraction

EEMS for all treatments and exposure times were analyzed, by subtracting the NT from the treated samples (Fig. 5). Representing all treatments in this way, allow us to have an overview of the effect caused by each UV treatment on the FDOM fingerprint. Therefore, applying this approach, it was possible to analyze individually the peaks affected by the treatments. Thus, we aim to address the practicality and efficiency of the UV microfluidic device, since within the short irradiation time we recorded specific FDOM/CDOM responses.

In general, this approach showed that specific peaks are predominant, specifically humic-like fluorophores, A (400–500 nm emission and 237–260 nm excitation), C (400–500 nm emission and 300–370 nm excitation) and protein-like fluorophore or fluorophore T (340–381 nm emission, 225–237 nm and 275 nm excitation). We observed that UVB treatment mainly modified the fluorophores A and C fingerprints. The greatest effect was recorded when applying the UVB for 60 min. This setup is characterized by showing the presence of a peak located in (EM/EX) = 500/250 nm, the main difference between treated and non-treated samples (Fig. 5 c). EEMS analysis of samples treated under the UVB for 30 and 90 min shows the presence of the A fluorophore, but with a low FI, Fig. 5 (b, d). Interestingly, fluorophore T shows an increase in its FI after UV treatment. This peak was detectable in the region according to an (EM/EX) range between 320 and 380/225–237 nm. Same peak intensities were recorded when UVB at 15 and 30 min were applied, but disappearing at 60 min, and reappearing with a change intensity (close to 200 A.U.) in the peak position.

Exposing the samples to UVA also exerts modifications on both fluorophores, namely peaks A and T. Fluorophore A shows a similar FI through all setups, Fig. 5 (e, f, g). We must notice that, after applying the UVA for 90 min treatment, the peak A signal was lost. Despite the small FI differences between the first three-time setups, a slight increase in the FI was recorded between UVA at 15 and 30 min, afterward a decrease in FI was recorded between UVA at 60 and 90 min, Fig. 5 (g, h). Furthermore, fluorophore T is detected in its two excitation positions, with an increasing intensity from UVA at 15 to 30 min, Fig. 5 (e, f). After applying longer irradiation times the peak T fades out, and a very low FI is detected for the irradiated samples under the UVA at 60 and 90 min treatments, Fig. 5 (g, h).

In general, the combined treatment shows a decrease in the FI in the region matching with peak A, this was observed in all treatments, especially in the combined at 90 min (Fig. 5 l). Fluorophore T appears at the 15 min mark, and then signal matching this peak is lost at 30 min, Fig. 5 (i, j). However, the peak is recorded once more in the combined at 60 and 90 min treatment, showing fluorophore T with its characteristic two excitation peaks, Fig. 5 (k, l).

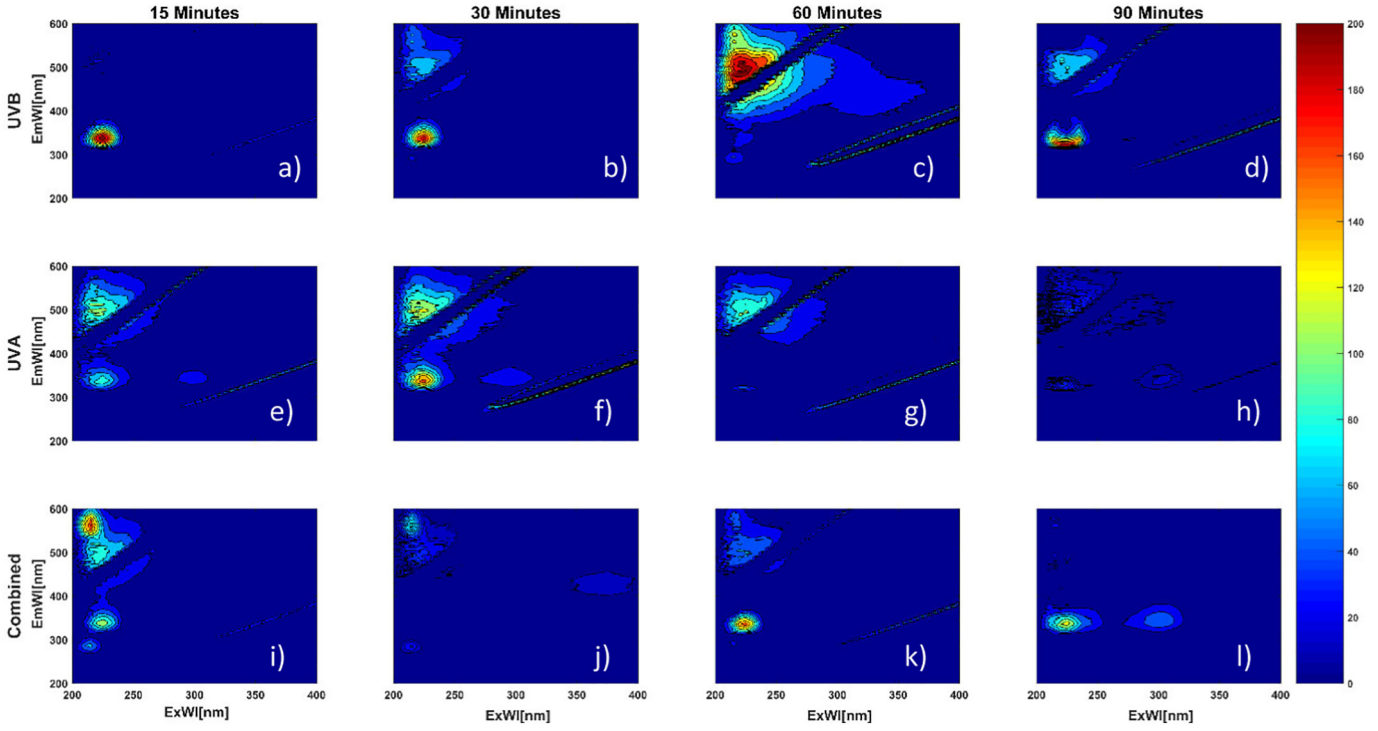

Fig. 5. - Overall view of subtraction of FI from non-treated to the treated of all treatments with a color bar in arbitrary units (A.U.). In the larger image, the rows and columns have the X-axis representing treatment time and the Y-axis showing the type of treatment used, with each square then having its X-axis (excitation) and Y-axis (emission), individually entitled from a to l.

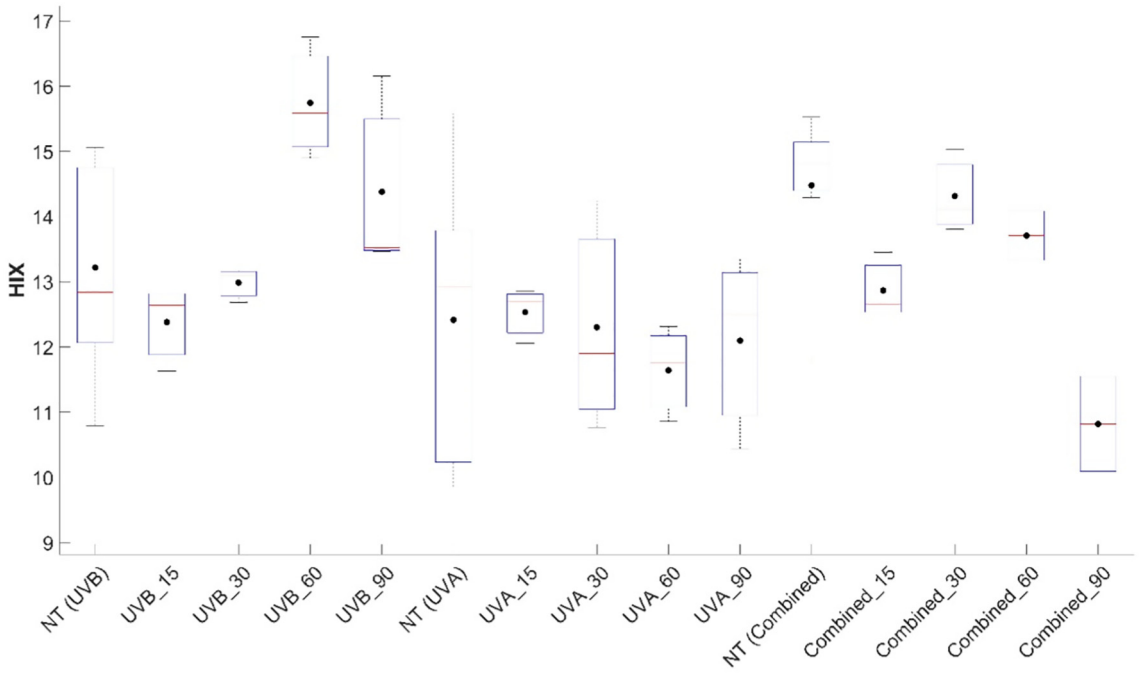

Fig. 6. – Humification Index from all treatments and respective NT. All values are above the 10 mark, indicating a strong humic character with an important terrigenous contribution. The black dot (•) represents the average, the red line (—) is the median, the top, and the bottom indicate the 25th and 75th quartile, the end of each whisker representing the maximum and the minimum value, respectively. (For interpretation of the references to color in this figure legend, the reader is referred to the web version of this article.)

3.3. HIX

In general, all recorded values were above 10, indicating an important humic character with a terrigenous contribution in the samples, and since the values are below 16, there is also a weak recent in situ production shown in Fig. 6 [25,35].

Considering the average HIX values in Fig. 6, at UVB 15 min (12.4) the sample shows a decrease in the humic compounds compared to NT (13.2), which then increases over irradiation time, with the highest point at 60 min (15.7). Though at UVB 90 min (14.4) there is a regression, it is still above the NT average.

Samples exposed to the UVA treatment, including NT, show average values between 12 and 13, except for UVA at 60 min with an 11.6 average. UVA at 15 min has the highest average value (12.5), followed by the NT (12.4), UVA 30 min (12.3) and 90 min (12.1). UVA treatment compared to UVB and combined shows a higher variation between replicas HIX values, with the NT being the most predominant.

In the combined treatment, all the average values are smaller than the corresponding NT. In this case, combined at 15 min (12.9) caused a dropped of 1.6 compared to the NT average value of 14.5, after which there is a recovery, almost reaching the same value as the NT, before decreasing again. Combined at 90 min (10.8) has the lowest average value of all treatments in the HIX.

4. Discussion

This research investigated the novelty of the UV irradiation extension, by presenting its design, uses and feasibility. Furthermore, we examined the CDOM/FDOM photodegradation dependence with a set of two UV irradiation sources and selected treatment times, applied with the developed device.

The efficiency of the developed UV microfluidic device was tested by applying selected setups combining temperature and UV radiation. We presented a working system, nevertheless the results obtained show a higher standard variation. This variation is more accentuated in the NT samples, which can be attributed to the variation of the spectrophotometer and the spectrofluorometer for each measurement and by the presence of air as well as changes in the NT sample through the days.

In order to test the capabilities of the microfluidic device, we performed specific tests with fresh filtered seawater samples. Absorption coefficients were calculated, and specific patterns were recorded in the slope coefficient occurring after 15 min of treatment. Calculated values tend to be smaller than those for respective NT samples, Fig. 4. The decrease in the slope ratio can be considered as caused by biodegradation of the sample in the first 15 min, followed by an increase, represented by photodegradation where the intensity depends on the type of radiation [17]. Thus, changes in the slope ratio, suggest an increase in dissolved organic carbon concentration, a shift from high to low molecular weight induced by photo- and biodegradation [17,36].

Moreover, the application of selected UV LED irradiation sources shows different outcomes. Samples exposed to UVB showed an increase in the slope ratio over time, while the combined and the UVA treatments both showed lower values. These similarities are explained by the influence of UVA in the combined treatment as the first irradiation applied, where the y-intercept is the distinguishing parameter between both treatments. This observation agrees with the energetic content of the radiation sources applied and its ability to induce photolysis of DOM compounds [37]. We could assume this similarity can also prove the reproducibility of the microdevice and that the influence of UVB after applying UVA is not significant in CDOM which is also confirmed by the EEMS subtraction.

In the present study FDOM response is specifically related to the UV radiation applied, as it was recorded for HIX and the EMMS subtraction, Figs. 5 and 6. As is shown in Fig. 5, the application of UVB treatment seemed to induce a release of humic-like compounds, which was confirmed by the increase in the FI values in the first steps of this treatment. Interestingly, the FI of this released fluorophore decreased until its intensity is lost after 90 min of treatment (UVB at 90 min). This agrees with the observed values for HIX previously discussed. Application of complementary treatments,

namely UVA and the combined one, showed a similar trend in FI values for the humic-like and protein-like fluorophores. The results showed that the FI values in both treatments were lower when compared with UVB treatment. Higher FI values for NT samples were expected when compared with the treated samples since the effect of photodegradation is a known fact for FDOM [14,38,39], however Fig. 5c showed the opposite trend. This pattern suggests that the release of a fluorophore happened while the UVB treatment was applied. An increase in FI was also reported by Kouassi and Zika [48], when samples were irradiated by a mercury line of 265.2, 280.4, 296.7 and 313 nm. Patel-Sorrentino et al. [49] showed similar results to the UVB treatment where the peak of intensity happened at around 50 min of irradiation in the air environment, suggesting 60 min will not be the peak of intensity. This result was commented as not understandable in since they considered a non-existent connection between the two. Allard et al. [46] concluded that UV irradiation decomposes humic substances, where a 254 nm wavelength was used for irradiation. In two previous researches, UVA has been reported as the main responsible for these transformations [40,41]. These reports converge in a common factor, the amount of energy contained by UVA and UVB induces specific FDOM responses, which agrees in general terms with our observations.

Simultaneously, by applying UV radiation in a controlled setup with our microdevice, we recorded unique changes in HIX values due to the selection of time setups, Fig. 6. UVB treatment showed a specific feature when UVB 60 min was applied, showing an apparent release of humic-like compounds in the sample. This feature agrees with the previously reported production of sunscreen-like compounds by microorganisms exposed to luminic stress [42]. Application of UVA treatment to fresh DOM samples showed a relatively weaker effect on HIX values, which is consistent with the amount of energy contained by this radiation. Nevertheless, a decreasing tendency was observed for this treatment, when compared to HIX values against the respective values for NT samples. Furthermore, these changes in HIX values suggest a change in the composition of the samples after treatment, where radiation type is considered as the main cause of this alteration in the origin of those compounds.

5. Conclusion

The presented microdevice with its novel UV structure showed its feasibility. By applying it to a DOM sample, we were able to induce photochemical changes in CDOM/FDOM. Treatment results exhibited behaviors comparable to previous studies, where time and type of radiation are directly related to the degree of degradation. Furthermore, UVB demonstrated a higher effect in the photodegradation, plus we observed a possible connection between UVB and humic-like compounds. By applying strictly controlled variables in selected setups, our experimental device enhances capacities in addressing biogeochemical processes in the marine environment, which were not accessible with conventional bulk methods. Thus, the new device allows for the investigation of photodegradation and the isolation of CDOM/FDOM responses contained in filtered seawater samples.

Enhancing of methodological capabilities of established (here optical) instrumentation can be achieved by different treatments prior to the original sampling. This can go from simple filtration to ultrasonic or heat exposures or, like in this study, the exposure to different UV irradiations. The volume that needs to be treated is a critical component, as typically one likes to expose quickly and with high energies, in all cases under controlled conditions. Here, we successfully utilized a microfluidic device for sample treatment, as it provides very good control overexposure of the sample. For future application, it makes sense a) to miniaturize the surrounding infrastructure to operate the microfluidic device and b) to transform it into a submersible, in situ applicable sample treatment. In combination with commercial optical sensors and autonomous platforms, microfluidic sample (pre-) treatment can enlarge the areas of application for aquatic DOM processes, marine hazard detections [43], or even be transformed into affordable mobile sensory instrumentation [26,44,45] encouraging citizens participation in science.

Acknowledgments

This study was carried out in the framework of the Ph.D. research training group “The Ecology of Molecules” (EcoMol) supported by the Lower Saxony Ministry for Science and Culture.

DFKI acknowledges financial support by the MWK through “Niedersachsen Vorab” (ZN3480).

M. L. Miranda acknowledges DAAD for the research scholarship (Forschungsstipendien für Doktoranden und Nachwuchswissenschaftler für mehr als 6 Monate, 2014/15, Number 57076385) and SENACYT-IFARHU for the research scholarship (for Doctoral and Postdoctoral studies 2017/18, Program BIPD-2016).

Authorship statement

Raquel Lopes: Conceptualization, Methodology, Validation, Formal analysis, Investigation, Data Curation, Writing - Original Draft, Writing - Review & Editing, Project administration. M. L. Miranda: Writing - Original Draft, Writing - Review & Editing, Validation, Supervision, Project administration. H. Schütte: Methodology, Resources. S. Gassmann: Conceptualization, Methodology, Resources, Writing - Original Draft, Writing - Review & Editing, Supervision, Project administration, Funding acquisition. O. Zielinski: Conceptualization, Resources, Writing - Original Draft, Writing - Review & Editing, Validation, Supervision, Project administration, Funding acquisition.

Declaration of competing interest

The authors declare that they have no known competing financial interests or personal relationships that could have appeared to influence the work reported in this paper.

Appendix A

Table 1
- Treatments setups for UV treatment.

Treatment	Combined		UVA	UVB
UV LED wavelength (nm)	340	280	340	280
Time (minutes)	15	15	15	15
	30	30	30	30
	60	60	60	60
	90	90	90	90

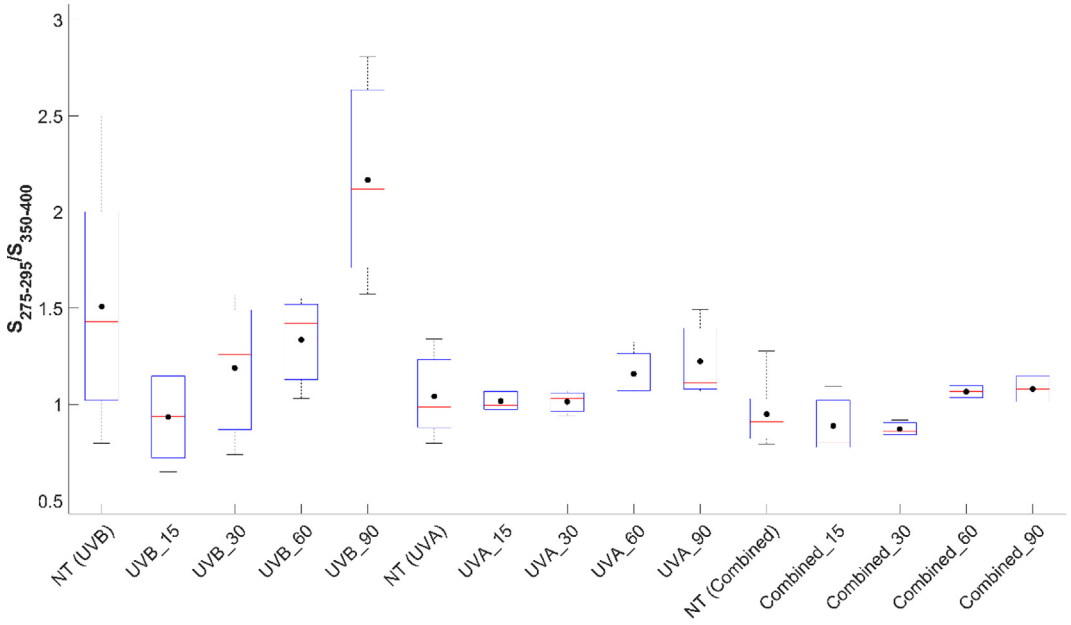

Fig. Apx 1. – Variation of the slope ratio from all treatments and respective NT. The black dot (•) represents the average, the red line (—) is the median, the top, and the bottom indicate the 25th and 75th quartile, the end of each whisker representing the maximum and the minimum value, respectively.

References

[1] J.P. Kutter, H. Klank, Microfluidics– Theoretical aspects, Microsystem Engineering of Lab-on-a-Chip Devices 2003, pp. 13–37.

[2] N.-T. Nguyen, S.A.M. Shaegh, N. Kashaninejad, D.-T. Phan, Design, fabrication and characterization of drug delivery systems based on lab-on-a-chip technology, Adv. Drug Deliv. Rev. 65 (11—12) (2013) 1403–1419, https://doi.org/10.1016/j.addr.2013.05.008.

[3] B.E. Rapp, Introduction, Microfluidics: Modelling, Mechanics and Mathematics 2017, pp. 3–7.

[4] J. Wang, Lab-on-valve mesofluidic analytical system and its perspectives as a "world-to-chip" front-end, Anal. Bioanal. Chem. 381 (4) (2005) 809–811, https://doi.org/10.1007/s00216-004-2920-7.

[5] G.M. Whitesides, The origins and the future of microfluidics, Nature 442 (7101) (2006) 368–373, https://doi.org/10.1038/nature05058.

[6] J. Watson, Subsea imaging and vision: An introduction, Subsea Optics and Imaging 2013, pp. 17–34.

[7] O. Zielinski, Subsea optics: An introduction, Subsea Optics and Imaging 2013, pp. 3–16.

[8] P.G. Coble, Characterization of marine and terrestrial DOM in seawater using excitation-emission matrix spectroscopy, Mar. Chem. 51 (4) (1996) 325–346, https://doi.org/10.1016/0304-4203(95)00062-3.

[9] K. Kalle, Zum Probleme der Meereswasserfarbe, Ann. Hydrol. Mar. Mitt. 66 (1938) 1–13.

[10] R. Del Vecchio, N.V. Blough, Photobleaching of chromophoric dissolved organic matter in natural waters: kinetics and modeling, Mar. Chem. 78 (4) (2002) 231–253, https://doi.org/10.1016/s0304-4203(02)00036-1.

[11] M.L. Miranda, N.I.H. Mustaffa, T.B. Robinson, C. Stolle, M. Ribas-Ribas, O. Wurl, O. Zielinski, Influence of solar radiation on biogeochemical parameters and fluorescent dissolved organic matter (FDOM) in the sea surface microlayer of the southern coastal North Sea, Elementa-Sci. Anthrop. 6 (2018)https://doi.org/10.1525/elementa.278.

[12] J. Para, P.G. Coble, B. Charrière, M. Tedetti, C. Fontana, R. Sempéré, Fluorescence and absorption properties of chromophoric dissolved organic matter (CDOM) in coastal surface waters of the northwestern Mediterranean Sea, influence of the Rhône River, Biogeosciences 7 (12) (2010) 4083–4103, https://doi.org/10.5194/bg-7-4083-2010.

[13] P.G. Coble, Marine optical biogeochemistry: the chemistry of ocean color, Chem. Rev. 107 (2) (2007) 402–418, https://doi.org/10.1021/cr050350+.

[14] B.D. Downing, B.A. Pellerin, B.A. Bergamaschi, J.F. Saraceno, T.E.C. Kraus, Seeing the light: the effects of particles, dissolved materials, and temperature on in situ measurements of DOM fluorescence in rivers and streams, Limnol. Oceanogr. Methods 10 (10) (2012) 767–775, https://doi.org/10.4319/lom.2012.10.767.

[15] M. Miranda, A. Trojzuck, D. Voss, S. Gassmann, O. Zielinski, Spectroscopic evidence of anthropogenic compounds extraction from polymers by fluorescent dissolved organic matter in natural water, J. Eur. Opt. Soc. Rapid Publ. 11 (2016)https://doi.org/10.2971/jeos.2016.16014.

[16] J.R. Helms, A. Stubbins, J.D. Ritchie, E.C. Minor, D.J. Kieber, K. Mopper, Absorption spectral slopes and slope ratios as indicators of molecular weight, source, and photobleaching of chromophoric dissolved organic matter, Limnol. Oceanogr. 53 (3) (2008) 955–969, https://doi.org/10.4319/lo.2008.53.3.0955.

[17] P. Li, J. Hur, Utilization of UV-Vis spectroscopy and related data analyses for dissolved organic matter (DOM) studies: a review, Crit. Rev. Environ. Sci. Technol. 47 (3) (2017) 131–154, https://doi.org/10.1080/10643389.2017.1309186.

[18] N. Hudson, A. Baker, D. Reynolds, Fluorescence analysis of dissolved organic matter in natural, waste and polluted waters—a review, River Res. Appl. 23 (6) (2007) 631–649, https://doi.org/10.1002/rra.1005.

[19] E. Baszanowska, O. Zielinski, Z. Otremba, H. Toczek, Influence of oil-in-water emulsions on fluorescence properties as observed by excitation-emission spectra, J. Eur. Opt. Soc. Rapid Publ. 8 (2013)https://doi.org/10.2971/jeos.2013.13069 (doi:ARTN 13069).

[20] C. Moore, A. Barnard, P. Fietzek, M.R. Lewis, H.M. Sosik, S. White, O. Zielinski, Optical tools for ocean monitoring and research, Ocean Sci. 5 (4) (2009) 661–684, https://doi.org/10.5194/os-5-661-2009.

[21] V. Drozdowska, W. Freda, E. Baszanowska, K. Rudź, M. Darecki, J.R. Heldt, H. Toczek, Spectral properties of natural and oil polluted Baltic seawater — results of measurements and modelling, Eur. Phys. J-Spec. Top. 222 (9) (2013) 2157–2170, https://doi.org/10.1140/epjst/e2013-01992-x.

[22] N. Senesi, T.M. Miano, M.R. Provenzano, G. Brunetti, Characterization, differentiation, and classification of humic substances by fluorescence spectroscopy, Soil Sci. 152 (1991) 259–271, https://doi.org/10.1097/00010694-199110000-00004.

[23] E. Zhi, H. Yu, L. Duan, L. Han, L. Liu, Y. Song, Characterization of the composition of water DOM in a surface flow constructed wetland using fluorescence spectroscopy coupled with derivative and PARAFAC, Environ. Earth Sci. 73 (9) (2015) 5153–5161, https://doi.org/10.1007/s12665-015-4148-6.

[24] V. Drozdowska, P. Kowalczuk, M. Jozefowicz, Spectrofluorometric characteristics of fluorescent dissolved organic matter in a surface microlayer in the southern Baltic coastal waters, J. Eur. Opt. Soc. Rapid Publ. 10 (2015)https://doi.org/10.2971/jeos.2015.15050.

[25] A. Huguet, L. Vacher, S. Relexans, S. Saubusse, J.M. Froidefond, E. Parlanti, Properties of fluorescent dissolved organic matter in the Gironde estuary, Org. Geochem. 40 (6) (2009) 706–719, https://doi.org/10.1016/j.orggeochem.2009.03.002.

[26] A. Friedrichs, J.A. Busch, H.J. van der Woerd, O. Zielinski, SmartFluo: a method and affordable adapter to measure chlorophyll a fluorescence with smartphones, Sensors (Basel) 17 (4) (2017)https://doi.org/10.3390/s17040678.

[27] A. Friedrichs, O. Ferdinand, M.L.M. Montenegro, O. Zielinski, *SmartFluo goes FDOM: Advancement of the DIY fluorometer approach towards UV excitation.* Paper Presented at the OCEANS 2017 - Aberdeen, Aberdeen, UK, http://ieeexplore.ieee.org/document/8084741/ 2017.

[28] R. Röttgers, C. Häse, R. Doerffer, Determination of the particulate absorption of microalgae using a point-source integrating-cavity absorption meter: verification with a photometric technique, improvements for pigment bleaching, and correction for chlorophyll fluorescence, Limnol. Oceanogr. Methods 5 (1) (2007) 1–12, https://doi.org/10.4319/lom.2007.5.1.

[29] J. Wollschläger, R. Röttgers, W. Petersen, O. Zielinski, Stick or dye: evaluating a solid standard calibration approach for point-source integrating cavity absorption meters (PSICAM), Front. Mar. Sci. 5 (2019)https://doi.org/10.3389/fmars.2018.00534.

[30] A. Makarewicz, P. Kowalczuk, S. Sagan, M.A. Granskog, A.K. Pavlov, A. Zdun, ... M. Zabłocka, Characteristics of chromophoric and fluorescent dissolved organic matter in the Nordic Seas, Ocean Science 14 (3) (2018) 543–562, https://doi.org/10.5194/os-14-543-2018.

[31] J. Pearlman, O. Zielinski, A new generation of optical systems for ocean monitoring matrix fluorescence for Multifunctional Ocean sensing, Sea Technol. 58 (2) (2017) 30–33.
[32] R. Lopes, H. Schütte, M.L. Miranda, S. Gassmann, O. Zielinski, *Technology to avoid leaching in a microfluidic water sample treatment system.* Paper Presented at the ACTUATOR 2018; 16th International Conference on New Actuators, Bremen, 2018.
[33] I.R.G. Ogilvie, V.J. Sieben, C.F.A. Floquet, R. Zmijan, M.C. Mowlem, H. Morgan, Reduction of surface roughness for optical quality microfluidic devices in PMMA and COC, J. Micromech. Microeng. 20 (6) (2010)https://doi.org/10.1088/0960-1317/20/6/065016.
[34] S.A. Green, N.V. Blough, Optical absorption and fluorescence properties of chromophoric dissolved organic matter in natural waters, Limnol. Oceanogr. 39 (8) (1994) 1903–1916, https://doi.org/10.4319/lo.1994.39.8.1903.
[35] A. Zsolnay, E. Baigar, M. Jimenez, B. Steinweg, F. Saccomandi, Differentiating with fluorescence spectroscopy the sources of dissolved organic matter in soils subjected to drying, Chemosphere 38 (1) (1999) 45–50, https://doi.org/10.1016/s0045-6535(98)00166-0.
[36] A.M. Hansen, T.E.C. Kraus, B.A. Pellerin, J.A. Fleck, B.D. Downing, B.A. Bergamaschi, Optical properties of dissolved organic matter (DOM): effects of biological and photolytic degradation, Limnol. Oceanogr. 61 (3) (2016) 1015–1032, https://doi.org/10.1002/lno.10270.
[37] D. Karentz, M. Bothwell, R. Coffin, A. Hanson, G. Herndl, S. Kolham, R. Wetzel, et al., Impact of UV-B radiation on pelagic freshwater ecosystems: report of working group on bacteria and phytoplankton, Ergebnisse Der Limnologie 43 (1994) 31.
[38] J.R. Lakowicz, Principles of Fluorescence Spectroscopy, 3 ed., 2006.
[39] R.G. Zepp, W.M. Sheldon, M.A. Moran, Dissolved organic fluorophores in southeastern US coastal waters: correction method for eliminating Rayleigh and Raman scattering peaks in excitation–emission matrices, Mar. Chem. 89 (1–4) (2004) 15–36, https://doi.org/10.1016/j.marchem.2004.02.006.
[40] H. De Haan, Solar UV-light penetration and photodegradation of humic substances in peaty lake water, Limnol. Oceanogr. 38 (5) (1993) 1072–1076, https://doi.org/10.4319/lo.1993.38.5.1072.
[41] J. Hur, K.Y. Jung, Y.M. Jung, Characterization of spectral responses of humic substances upon UV irradiation using two-dimensional correlation spectroscopy, Water Res. 45 (9) (2011) 2965–2974, https://doi.org/10.1016/j.watres.2011.03.013.
[42] Q. Gao, F. Garcia-Pichel, Microbial ultraviolet sunscreens, Nat. Rev. Microbiol. 9 (11) (2011) 791–802, https://doi.org/10.1038/nrmicro2649.
[43] O. Zielinski, J.A. Busch, A.D. Cembella, K.L. Daly, J. Engelbrektsson, A.K. Hannides, H. Schmidt, Detecting marine hazardous substances and organisms: sensors for pollutants, toxins, and pathogens, Ocean Sci. 5 (3) (2009) 329–349, https://doi.org/10.5194/os-5-329-2009.
[44] J. Busch, R. Bardaji, L. Ceccaroni, A. Friedrichs, J. Piera, C. Simon, ... O. Zielinski, Citizen Bio-Optical Observations from Coast- and Ocean and Their Compatibility with Ocean Colour Satellite Measurements, Remote Sensing 8 (11) (2016)https://doi.org/10.3390/rs8110879.
[45] L. Ceccaroni, J. Piera, M.R. Wernand, O. Zielinski, J.A. Busch, H.J. Van Der Woerd, ... K. Dubsky, Citclops: A next-generation sensor system for the monitoring of natural waters and a citizens' observatory for the assessment of ecosystems' status, PLoS One 15 (3) (2020), e0230084. https://doi.org/10.1371/journal.pone.0230084.
[46] B. Allard, H. Borén, C. Pettersson, G. Zhang, Degradation of humic substances by UV irradiation, Environ. Int. 20 (1) (1994) 97–101, https://doi.org/10.1016/0160-4120(94)90072-8.
[47] S. Gassmann, A. Trozjuk, J. Singhal, H. Schuette, M.L. Miranda, O. Zielinski, PCB based micro fluidic system for thermal cycling of seawater samples, Paper Presented at the 2015 IEEE International Conference on Industrial Technology (ICIT), Seville, Spain, 2015.
[48] A.M. Kouassi, R.G. Zika, Light-induced alteration of the photophysical properties of dissolved organic matter in seawater part I. Photoreversible properties of natural water fluorescence, Neth. J. Sea Res. 27 (1) (1990) 25–32, https://doi.org/10.1016/0077-7579(90)90031-b.
[49] N. Patel-Sorrentino, S. Mounier, Y. Lucas, J.Y. Benaim, Effects of UV-visible irradiation on natural organic matter from the Amazon basin, Sci. Total Environ. 321 (1–3) (2004) 231–239, https://doi.org/10.1016/j.scitotenv.2003.08.017.
[50] S. Shen, Y. Li, S. Wakida, Characterization of dissolved organic carbon at low levels in environmental waters by microfluidic-chip-based capillary gel electrophoresis with a laser-induced fluorescence detector, Environ. Monit. Assess. 166 (1–4) (2010) 573–580, https://doi.org/10.1007/s10661-009-1024-4.
[51] O. Zielinski, N. Rüssmeier, O. Ferdinand, M. Miranda, J. Wollschläger, Assessing fluorescent organic matter in natural waters: towards in situ excitation–emission matrix spectroscopy, Appl. Sci. 8 (12) (2018)https://doi.org/10.3390/app8122685.